ELSEVIER

Journal of Fluids and Structures 25 (2009) 1213–1235

JOURNAL OF FLUIDS AND STRUCTURES

www.elsevier.com/locate/jfs

Fluid-elastic instability in tube arrays subjected to air-water and steam-water cross-flow

D. Mitra[1], V.K. Dhir*, I. Catton

Department of Mechanical and Aerospace Engineering, University of California at Los Angeles, Los Angeles, CA 90095, USA

Received 9 March 2009; accepted 9 July 2009
Available online 25 August 2009

Abstract

Flow induced vibrations in heat exchanger tubes have led to numerous accidents and economic losses in the past. Efforts have been made to systematically study the cause of these vibrations and develop remedial design criteria for their avoidance. In this research, experiments were systematically carried out with air-water and steam-water cross-flow over horizontal tubes. A normal square tube array of pitch-to-diameter ratio of 1.4 was used in the experiments. The tubes were suspended from piano wires and strain gauges were used to measure the vibrations. Tubes made of aluminum; stainless steel and brass were systematically tested by maintaining approximately the same stiffness in the tube-wire systems. Instability was clearly seen in single phase and two-phase flow and the critical flow velocity was found to be proportional to tube mass. The present study shows that fully flexible arrays become unstable at a lower flow velocity when compared to a single flexible tube surrounded by rigid tubes. It is also found that tubes are more stable in steam-water flow as compared to air-water flow. Nucleate boiling on the tube surface is also found to have a stabilizing effect on fluid-elastic instability.

Keywords: Fluid-elastic instability; Flow induced vibration; Two-phase flow; Air-water flow; Steam-water flow

1. Introduction

Flow-induced vibrations in heat exchangers have been a major cause of concern in the nuclear industry for several decades. Many incidents of failure of heat exchangers due to apparent flow-induced vibration have been reported through the USNRC incident reporting system. Some examples of tube failures in commercial steam generators are reported in the review by Pettigrew and Taylor (1991). The phenomenon has been studied since the 1970s and the database of experimental studies on flow-induced vibration is constantly updated with new findings and improved design criteria for heat exchangers. Shell and tube type heat exchangers experience flow-induced vibration due to high velocity flow over the tube banks. Flow-induced vibration in these structures is caused by three mechanisms: vortex shedding that leads to vibration due to vortices shed when a fluid flows over a bluff structure, fluid-elastic instability where vibrations are caused as a result of the competition between the energy input by the fluid and the energy expended in damping by the structure, and turbulent buffeting.

*Corresponding author. Tel.: +1 310 825 9617; fax: +1 310 206 4830.
E-mail addresses: dmitra@ucla.edu (D. Mitra), vdhir@seas.ucla.edu (V.K. Dhir), catton@ucla.edu (I. Catton).
[1]Currently at Surefire LLC, Fountain Valley, CA, USA.

0889-9746/$ - see front matter
doi:10.1016/j.jfluidstructs.2009.07.002

Connors (1970) attributed fluid-elastic instability to fluid forces induced by the displacement of tubes and their interaction and proposed an instability map based on a dimensionless velocity parameter known as the reduced velocity and a dimensionless structural parameter known as the mass damping parameter, thus giving rise to the Connors' criterion that is still commonly used for presenting results of fluid-elastic instability. Such a correlation is suggested by a dimensional analysis of the governing parameters and takes the form

$$\frac{V_{p,\mathrm{cr}}}{fD} = K\left(\frac{2\pi m\zeta}{\rho D^2}\right)^b, \tag{1}$$

where $V_{p,\mathrm{cr}}$ is the critical pitch or gap velocity of the fluid, f is the natural frequency of the tube, D is the outer diameter, m is the mass per unit length of the tube and includes the added mass of the fluid, ζ is the total damping ratio of the tube, and ρ is the fluid density. The proportionality constant K and exponent b are coefficients obtained by fitting experimental data. Experiments have shown that b is typically around 0.5 (Pettigrew and Taylor, 1991). K is the instability constant that varies as a function of the pitch-to-diameter ratio and array geometry. It should be noted that the Connors criterion fails to completely explain the mechanism of fluid-elastic instability. In two-phase flow, void fraction and flow regime, which are not explicitly represented in Connors' criterion, also affect the instability.

Visual observation of tube motion in single phase flow was made by Chen and Jendrzejcyk (1981). They observed the motion of the tubes in an array in synchronous orbits. Lever and Weaver (1986) showed that relative motion of tubes was not necessary for fluid-elastic instability except for cases where neighboring tubes were very slightly detuned from each other. More recently, Adinolfi (2003) observed in his experiments that the motion of the tubes was uncorrelated and showed no specific order.

Most of the early work on fluid-elastic instability was carried out with single-phase fluids such as air or water due to the simpler nature of the experiments. Most recently, Schroder and Gelbe (1999) provided design guidelines for single phase flow based on an experimental data bank consisting of about 300 data points. Their design criterion for the instability threshold is based on statistical measures in the data scatter and reveal a dependence of the factors K and b on the pitch to diameter ratio of the tube array and also the geometric arrangement of the array.

A lot of experimental research in two-phase flow has been carried out with air-water flow systems. These experiments have been carried out with different tube pitch-to-diameter ratios, array geometries and tube suspension methods. A few experiments have been carried out with steam-water flow and more recently with freon flow. Developments in flow-induced vibration in heat exchangers have been reviewed by Weaver and Fitzpatrick (1988), Pettigrew and Taylor (1991, 1994), Pettigrew et al. (1998) and Weaver et al. (2000). Some of the experimental work in air-water, steam-water and Freon flow are briefly reviewed here. The experiments of Heilker and Vincent (1981) suggested a value of 5 for the instability constant, K. The experiments of Remy (1982) did not yield any values of the instability constant for two-phase flow cases, but suggested a value of 1.17 for the combined parameter $K\sqrt{2\pi\zeta}$ in single-phase flow.

Pettigrew et al. (1985, 1989) conducted comprehensive experiments in air-water flow pertaining to nuclear applications. They tested normal square, rotated square, normal triangular, and parallel triangular arrays of cantilevered tubes having a P/D ratio of 1.47 and 1.32. Tests were conducted with an all flexible tube array and a single flexible tube in a rigid array. Damping ratio was measured at half the mass flux required for instability. Their experimental results suggest a value of 4 for K. The critical reduced velocities were lower for a fully flexible array as compared to a single flexible tube in an array. The authors also found an effect of the P/D ratio on the slope of the instability curve indicated by the value of the constant, K. This effect was more pronounced in two-phase flow cases and was attributed to hydrodynamic coupling enhanced by confinement. They also concluded that in the intermittent flow regimes at void fractions higher than about 80%, calculated based on a homogeneous equilibrium model, instability was achieved at lower values of critical velocity than would be predicted using the Connors' criterion. The effect of the geometry of the tube array on tube vibration was recently investigated by Pettigrew et al. (2001). Their experiments revealed an effect of both the pitch-to-diameter ratio and the array geometry on the instability constant K. The effect was most pronounced with the rotated triangular array.

Joo (1994) and Joo and Dhir (1994, 1995) investigated fluid-elastic instability in air-water flow and proposed a mechanistic model for the instability based on the forces acting on the tube. They proposed a different mechanism where the onset of instability was attributed to a decrease in the effective stiffness of the tubes, rather than a mechanism of negative damping proposed by other researchers. Their work places emphasis on the stiffness of the tubes, which is a function of the tube suspension method. Though steam-water flow represents the true situation in a heat exchanger, two-phase fluid-elastic instability experiments in steam-water flow are not carried out extensively due to the complexity and the expense involved. However, several major parameters such as density ratio, viscosity ratio, surface tension, and compressibility differ in steam-water flow as compared to air-water flow. Feenstra et al. (2002) point out some of these differences and stress on the need to determine the effect of these differences.

Axisa et al. (1984) were among the first researchers to conduct air-water and steam-water tests in their experimental test facility. Instability was seen in both air-water and steam-water flow cases. Damping ratios were similar in both steam-water and air-water flow and showed a strong dependence on the void fraction. The authors extended their work to triangular arrays in a subsequent work (Axisa et al., 1985) and found similar behavior for both square and triangular arrays. This is in contradiction to the results of Pettigrew et al. (1989) who found a dependence of the instability on the geometry of the tube array.

Nakamura et al. (1995) presented a new theory for correlating the instability data based on equating the energy of the fluid to that of the tube oscillation in steam-water flow. Recently, the same group (Nakamura et al., 2002; Hirota et al., 2002; Mureithi et al., 2002) has completed a series of tests providing some much needed data on damping and fluid-elastic instability in steam-water two-phase flow. Their results indicate that the critical reduced velocity decreased with an increase in system pressure of the steam-water mixture. However, the critical reduced velocity did not change significantly with void fraction.

Apart from steam-water flow, experiments have also been carried out with freon. Feenstra et al. (2000, 2002) carried out experiments using Freon as the working fluid. Their objective was to develop a methodology for predicting critical velocities for fluid-elastic instability based on the physics of the phenomenon. This was driven by the fact that their instability data when plotted on Connors' criterion did not show a strong dependence on the mass damping parameter. The contribution of this paper was a new method for calculating the average density of the mixture and an equivalent energy weighted flow velocity using a newly developed void fraction model that allowed for slip. This was followed by a subsequent study (Feenstra et al., 2003) where the authors used their newly developed model to recast the two-phase flow data of various researchers. Their results show that the new model indeed collapsed their data with the other researchers thus providing a new way of plotting the flow instability maps in two-phase flow.

Pettigrew et al. (2002) present a comparison of results of tests conducted in air-water, Freon 22 and Freon 134a two-phase cross-flow with a rotated triangular tube array. The damping values obtained were found to be similar in air-water and two-phase flow of freon in spite of the different physical properties of the two fluids prompting the authors to point out the need for a better understanding of the principal parameters such as surface tension governing damping in two-phase flow. They also suggest studying the detailed characteristics of flow regimes between the tubes for the two fluid systems considered.

In summary, a review of the experimental database in two-phase fluid-elastic instability reveals large scatter in the data when plotted on the Connors' criterion map. While some of these differences are expected and attributed to differences in the method of calculation of the parameters controlling instability, some others are related to differences in fluid and structural properties that do not directly appear in the criterion. The manner in which these parameters such as the tube suspension method and fluid properties including drag and lift forces, density, viscosity, and compressibility affect the instability is not well understood. The objective of the present research is to conduct systematic experiments in air-water and steam-water flow with the same experimental setup and investigate the differences or similarities between the two fluid systems with respect to the onset of fluid-elastic instability. The effect of nucleate boiling in altering the onset of fluid-elastic instability is also investigated.

2. Experimental set-up

A schematic of the flow loop and the test section used to conduct the fluid-elastic instability experiments is shown in Fig. 1. Photographs are shown in Fig. 2. A centrifugal pump is used to pump de-ionized water from a 1.5 m^3 (400 gallon) tank through the test-section at a maximum flow rate of 6.3×10^{-3} m^3/s (100 gallons per minute) at 25 °C yielding a maximum free-stream velocity of 0.4 m/s. After passing through the test-section, the water or two-phase mixture is returned back into the reservoir tank. The temperature of the water in the reservoir is maintained constant by circulating chilled water through a copper cooling coil immersed in the reservoir. The entire flow loop and test section is thermally insulated to minimize heat losses.

A 210 kW inline heater is provided in the flow loop upstream of the test-section assembly to heat the water to saturation for steam-water flow runs. A turbine flow-meter is used to monitor the water flow rate. For the air-water flow experiments compressed air, regulated at an outlet pressure of 200 kPa (14 psig), is introduced into the mixing section to produce the two-phase mixture. The air flow rate is controlled using a needle valve and monitored using a turbine flowmeter. A maximum air flow rate of 7×10^{-3} m^3/s can be achieved in the test section. A correction is applied to the airflow rate since the pressure and temperature in the test section are different from that at the metering section.

Steam-water mixtures are generated using a combination of the inline heater and a smaller 1500 W control heater placed in the mixing section. This enables the production of steam by controlling the total power supplied to the heaters. Since the water immediately upstream of the control heater is always subcooled, an energy balance is performed

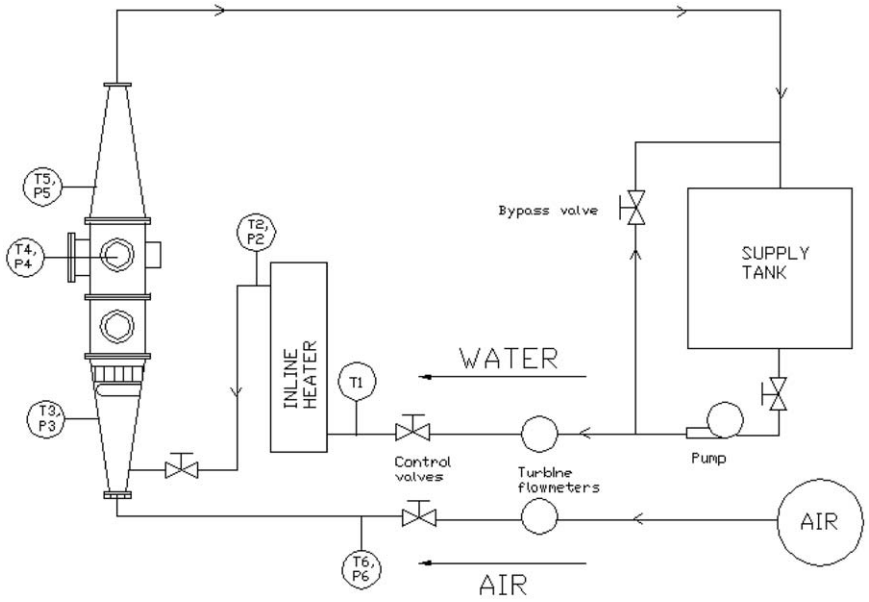

Fig. 1. Flow loop schematic for fluid-elastic instability experiments.

to determine the quality of the steam-water mixture in the test-section. Temperature and pressure at various locations in the flow loop are indicated by thermocouples and pressure transducers placed as shown in Fig. 1. The average operating pressures and temperatures, and the corresponding fluid properties in the test-section are listed in Table 1.

The test chamber consists of four sub-assemblies: mixing/entrance section, viewing section, test-section, and exit section. A schematic of each of the sections is shown in Fig. 3. Air is introduced into the mixing section from the bottom through an air-injection plate. For the air-water flow runs, air and water mix and flow vertically upwards through a honeycomb where the flow is straightened. The 1500 W control heater is installed immediately upstream of the honeycomb to produce steam during steam-water flow runs. The viewing section is used to make free-stream void fraction measurements in air-water flow experiments. This section also allows visualization of the two-phase flow before it enters the test tube bundle.

The test-section houses the rod bundle. A normal square array of tubes with pitch to diameter ratio of 1.4 is used in the experiments. The tubes have an outer diameter of 0.016 m and a length of 19 cm. Three different tube masses were tested in the experimental program as detailed in a later section on structural properties of tube arrays. The entire test-section has a cross section of $0.23\,\text{m} \times 0.09\,\text{m}$ (9.5 inches $\times$ 3.5 inches) and is 0.33 m (13 inches) in height. Dummy movable plates are installed in the test-section to provide a variable flow area. The plates are adjusted in the experiments such that the effective free-stream flow area in the test-section is $0.01596\,\text{m}^2$. The test-section houses a 5×3 fixed rod bundle and a 5×3 flexible one immediately downstream of the fixed bundle. The flexible tube array is suspended from the inner walls of the test section using stainless steel piano wires (0.51 mm diameter), details of which are presented in Fig. 4(a). Since the number of tube columns was limited to three in the 5×3 array, the complete effects of a fully flexible array may not be present in the experiments. Glass view ports are provided for visualization of the flow and the tubes as they vibrate. As the flow characteristics are expected to change due to phase change in steam-water flow, free-stream void fraction measurements were made through these view ports to reflect void-fractions just upstream of the tube bundle. Half cylinders are attached to the inner sidewalls of the test section to provide a uniform boundary condition at the walls of the test section. Some tests are conducted with a single flexible tube in which case rigid tubes are installed in place of the flexible tubes using the sidewalls as a support structure.

A tensioning mechanism is attached to one end of the piano wires to adjust the tension and thereby natural frequency of the tubes. Using this mechanism, the natural frequency of the tubes in the array can be adjusted to within ± 0.3 Hz of each other. The tube vibration response is measured using electrical resistance strain gauges. The strain gauges respond to change in applied strain and hence can be used as an indicator of tube vibration. Two strain gauges are bonded on opposite sides of a stainless steel shim (0.1 mm thick), which is then spot welded to the piano wire as shown in Fig. 4(b). The thickness of the shims is chosen such that the addition of the shim minimally alters the stiffness of the tube assembly. The strain gauges are connected in a half-bridge configuration and hence respond to only pure bending of the

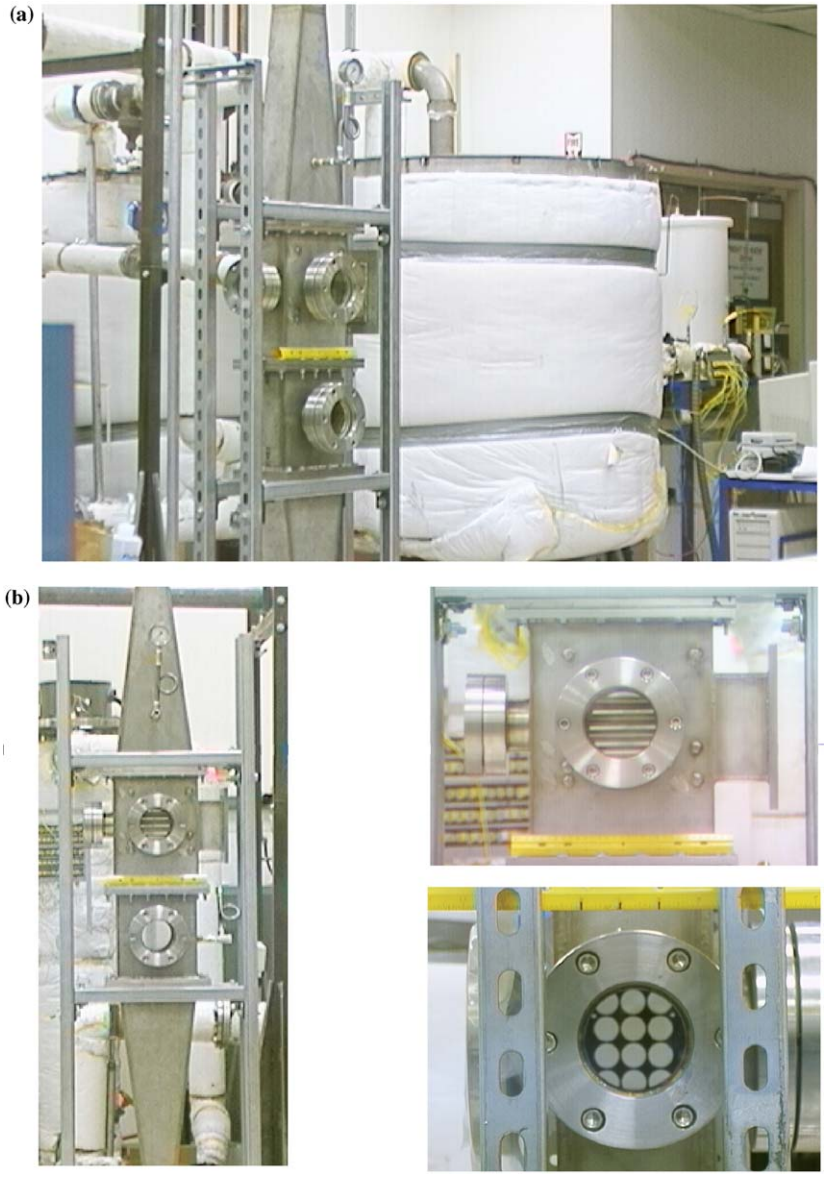

Fig. 2. Photographs of flow loop and test section. (a) Flow loop, (b) Test section assembly, (c) Test section (Half cylinders can be seen), (d) Test section (End view).

Table 1
Average fluid properties in test section.

Property	Air-water flow	Steam-water flow
Average pressure (kPa)	114	114
Average Temperature (°C)	25	103.4
Liquid density (kg/m^3)	998	956
Gas density (kg/m^3)	1.2	0.66
Surface tension (N/m)	0.072	0.059

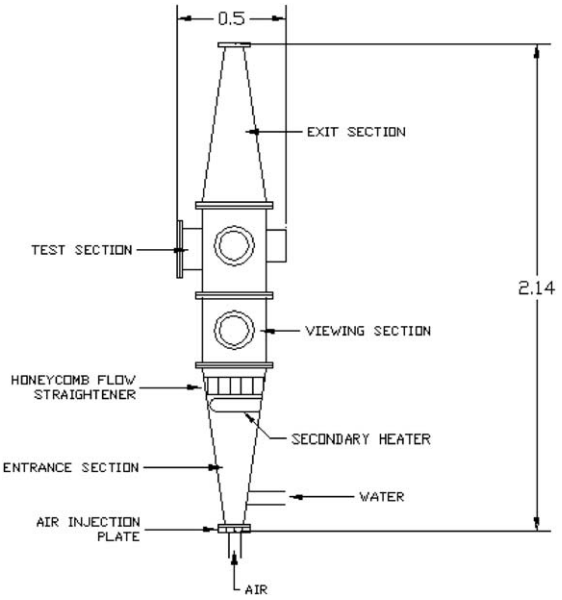

Fig. 3. Schematic of test chamber assembly (Dimension in meters).

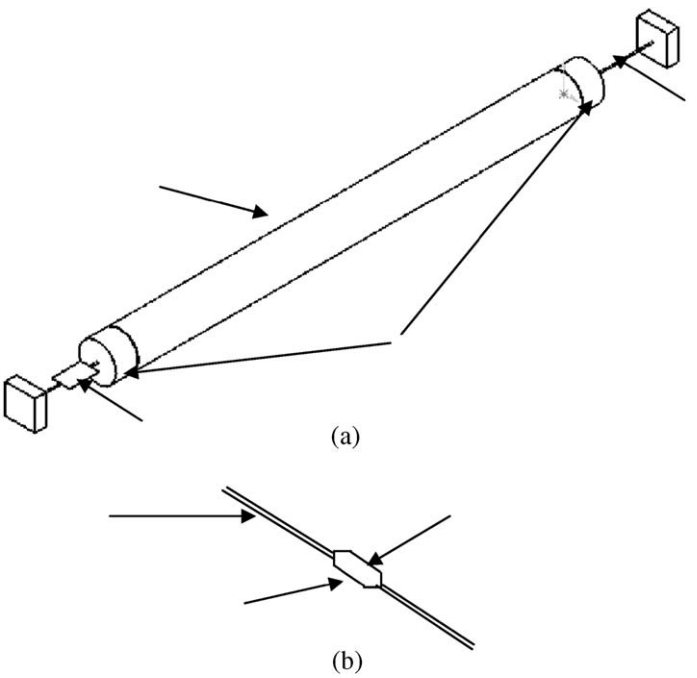

Fig. 4. (a) Schematic of test tube suspension; (b) Details of strain gauge mounting procedure.

shim or the piano wire. In order to protect the strain gauges from rapid degradation in the corrosive steam-water environment, the shim and the strain gauges are covered with highly flexible polyolefin shrink fit tubing.

Some experiments were carried out with nucleate boiling on the surface of a central flexible tube. For these experiments, two cylindrical 500 W cartridge heaters having a nominal diameter of 0.012 m were inserted inside a hollow brass tube of outer diameter 0.016 m and inner diameter 0.0125 m. Thermocouples placed diametrically opposite at a

total of six different locations on the outer surface of the tube yielded the tube surface temperature. A maximum heat flux of 11.2 W/cm^2 could be produced on the tube surface.

Chord averaged void fraction (α) measurements were made using a dual beam gamma densitometer (Cs 137 and Am 241). The gamma beam was collimated through a 2.54 cm diameter slit and the attenuated beam was incident on a NaI collector. The void fraction was measured using the radiation attenuation method. The sampling time was set at 100 s and was sufficiently large to capture any variations in the two-phase flow pattern that was essentially in the bubbly flow regime. At least five samples were averaged to yield the void fraction for a given liquid and gas flow rate.

3. Measurement methodology

In order to characterize the onset of fluid-elastic instability, the following measurement methodology is used. Free-stream superficial liquid flow velocity, V_l, is calculated using the formula

$$V_l = \frac{Q_l}{A}, \tag{2}$$

where Q_l is the liquid volume flow rate, and A is the cross section area upstream of the tube array. The liquid gap or pitch velocity, V_p, is calculated as

$$V_p = \frac{(P/D)}{(P/D-1)} V_l, \tag{3}$$

where P/D is the pitch-to-diameter ratio. In two-phase flow, the air flow rate is calculated from the turbine flowmeter measurements properly corrected for temperature and pressure. In steam-water flow, the vapor velocity is calculated from the mass quality, x, which in turn is determined from an energy balance in the test section. This yields the superficial free stream vapor velocity as

$$V_g = \frac{x}{1-x}\frac{\dot{m}_l}{\rho_g A}, \tag{4}$$

where $\dot{m}_l$ is the mass flow rate of the liquid, and ρ_g is the density of the vapor. The free-stream gas velocity corresponding to the critical void fraction is referred to as the critical superficial vapor velocity and is denoted $V_{g,\mathrm{cr}}$. The critical two-phase pitch velocity, to be used in the Connors' criterion, is then calculated as

$$V_{p,\mathrm{cr}} = (V_l + V_{g,\mathrm{cr}})\left(\frac{P/D}{P/D-1}\right). \tag{5}$$

From hereon, all liquid velocities are freestream liquid velocities and the total velocity is the pitch velocity of the two-phase fluid as defined in Eq. (5).

The two-phase equivalent density is calculated using the formula

$$\rho_{2\phi} = \alpha\rho_g + (1-\alpha)\rho_l, \tag{6}$$

where ρ_l and ρ_g are the liquid and gas phase densities and α is the void fraction.

The natural frequency of vibration is determined from the decay signal of tube vibration in still fluid and from the amplitude spectrum of the vibration response during flow conditions. The damping ratio is measured using the logarithmic decrement of amplitude in still fluid and using the amplitude spectrum in flow. In particular, the damping ratio, ζ, is naturally determined as a parameter of the vibration response equation (Pettigrew et al., 1989) fitted to the data of the amplitude spectrum of the vibration signal:

$$\frac{A_f}{A_O} = \left\{\left[1-\left(\frac{f}{f_n}\right)^2\right]^2 + 4\zeta^2\left(\frac{f}{f_n}\right)^2\right\}^{-1/2}. \tag{7}$$

In this equation, A_f is the intensity of the vibration amplitude at frequency f, and A_O is a constant that is proportional to the stiffness of the tube. Using this method, the total damping ratio in flow can be measured with an uncertainty of $\pm 16\%$.

The void fraction is measured from the attenuation of a gamma beam as

$$\alpha = \frac{\ln(I_\alpha) - \ln(I_l)}{\ln(I_g) - \ln(I_l)}, \tag{8}$$

where I is the intensity of the attenuated gamma beam, and I_l and I_g are the attenuation of the gamma beams in water and air respectively. The measured void fractions in air-water and steam-water flow were found to match the drift-flux correlation (Ishii and Zuber, 1979) given as

$$\alpha = \frac{V_g}{C_o(V_g + V_l) + V_{jg}}, \tag{9}$$

where α is the measured void fraction, C_o is the distribution parameter given by

$$C_o = 1.2 - 0.2\sqrt{\frac{\rho_g}{\rho_l}}, \tag{10}$$

and V_{jg} is the drift velocity given by

$$V_{jg} = 1.4\left[g\sigma\frac{(\rho_l - \rho_g)}{\rho_l^2}\right]^{0.25}; \tag{11}$$

in the above equation σ is the surface tension of water and g is the gravitational acceleration. Hence, this correlation with the parameters of Eqs. (10) and (11) was used to determine the void fraction during the actual experimental runs in lieu of the actual gamma beam attenuations. A validation of the experimentally measured void fraction using the gamma densitometers with the drift flux correlation is shown in Fig. 5 for superficial liquid flow velocities, V_l, of 0.24 and 0.16 m/s respectively.

The amplitude of tube vibration is expressed as a root mean square (rms) value of the strain gauge output signal in millivolts. The root mean squared value gives a representation of the vibration amplitude and can be used to compare the vibration amplitudes at different flow velocities. The rms amplitude is calculated as

$$A_{\text{rms}} = \sum_1^N (a_i - \bar{a})^2, \tag{12}$$

and the mean is expressed as

$$\bar{a} = \frac{1}{N}\sum_1^N a_i. \tag{13}$$

In these equations, a is the millivolt output and N represents the numbers of samples in the data set. The mean amplitude $\bar{a}$ also represents the steady static deflection of the tube in the downstream direction due to the drag force experienced by the tube. Hence, this value is subtracted from the rms value of the vibration amplitude.

Electronic data acquisition is performed using a National Instruments Data Acquisition Board for the strain gauge vibration signal. The strain gauge signal is sampled at a frequency of 200 Hz. The sampling rate is chosen to be about 10 times higher than the maximum frequency to be resolved. Temperature, pressure and flow rates are recorded at a lower sampling frequency of 1 Hz.

4. Structural properties of tube array

In the present work, the achievable liquid flow rate was limited to a small range due to limitations of the centrifugal pump used. Therefore, to obtain results over a wide range of mass damping parameters, tubes of three different masses were tested. Hollow aluminum and stainless steel tubes were tested along with a solid brass rod. The mass characteristics of the test tubes, frequency and damping ratio of a single tube in air and still water are provided in Table 2. The natural frequency of the tubes was determined by first tensioning the aluminum tube such that a clean vibration signal with a well defined logarithmic decay was obtained from the strain gauge signal. This was achieved at a vibration frequency of 21.4 Hz in air. Thereafter, the frequency of the other tube materials was chosen such that the stiffness of the tube-wire system was approximately constant. The stiffness of the tube-wire system was determined using the equation

$$k = 4\pi^2 f_a^2 M_a, \tag{14}$$

which is the equation for stiffness of a 1 degree-of-freedom vibrating spring-mass-damper system that was used to model the tube-wire system. In this equation, k is the stiffness of the tube-wire system; f_a and M_a are the natural frequency of tube vibration and tube mass in air. Using this approach, the frequencies of the different tube-wire systems

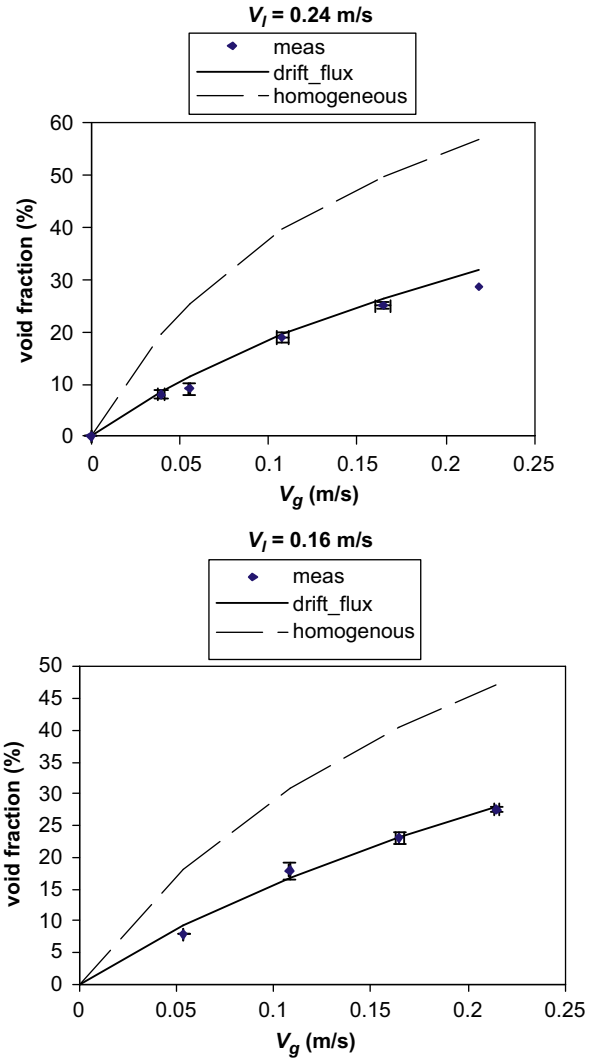

Fig. 5. Validation of experimentally measured void fraction in air-water flow at two different base freestream liquid flow rates and comparison with the homogenous equilibrium model.

Table 2
Structural properties of tubes used in fluid-elastic instability experiments.

Tube material	Mass in air (kg)	Mass per unit length (kg/m)	Natural frequency in air f_a (Hz)	Natural frequency in water f_l (Hz)	Damping ratio in air ζ_a (%)	Damping ratio in water ζ_l (%)
Hollow aluminum tube	0.0376	0.19	21.4	13.3	1.46	2.57
Hollow stainless steel tube	0.114	0.59	12.47	10.09	1.39	3.4
Solid brass tube	0.326	1.68	8.25	7.5	1.39	2.4
Solid brass rod with embedded heaters	0.257	1.35	9.71	8.65	1.47	2.45

were set such that the nominal stiffness of the aluminum and stainless steel tubes in air was about 690 N/m and that for the solid brass rod was 875 N/m. The damping ratio measurements in air and still water were calculated using the time decay of the vibration signal of the tube. It was observed that the frequency of the tubes in air decreased as the mass

increased in order to maintain constant system stiffness. The damping ratio in air was found to be around 1.4% for all three tube masses. The damping ratio in water increased for all three tubes.

In-flow damping ratios were measured using Eq. (7) for each two-phase flow experimental run at different void fractions. An example of the determination of the damping ratio in two-phase air-water flow is shown in Fig. 6 for a free-stream liquid velocity, V_l, of 0.16 m/s and a void fraction of 15%. The damping ratio is determined as the fitting parameter of the amplitude spectrum data of the vibration signal using Eq. (7). In fitting the data, maximum weights are given to the peak and tails. For a particular two-phase flow experiment, the damping ratio was found to increase with void fraction even beyond the instability point. In order to characterize the instability, the damping ratio corresponding to the critical void fraction was used. Joo and Dhir (1995) have used this approach to characterize instability in their experiments.

5. Air-water flow

Air-water two-phase flow experiments were carried out by holding the base liquid free-stream velocity, V_l, constant below the single phase instability limit while gradually increasing the air velocity in steps until large amplitude vibrations signaling fluid-elastic instability were observed. Using this method, experiments for each tube mass were conducted at base liquid freestream velocities of 0.24, 0.20 and 0.16 m/s. The objective of these experiments was to

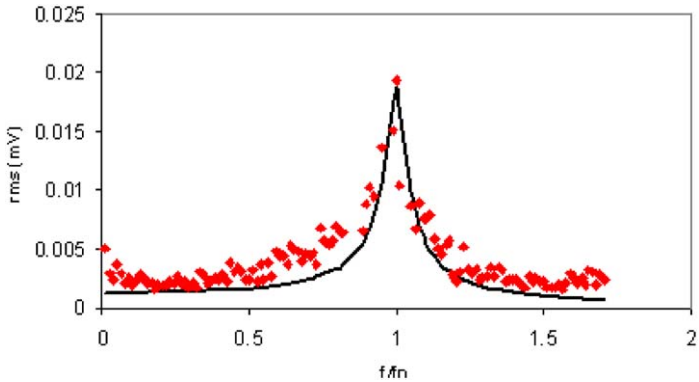

Fig. 6. Determination of damping ratio in two-phase air-water flow; $V_l = 0.16$ m/s; $\alpha = 15\%$; $\zeta = 3.32\%$.

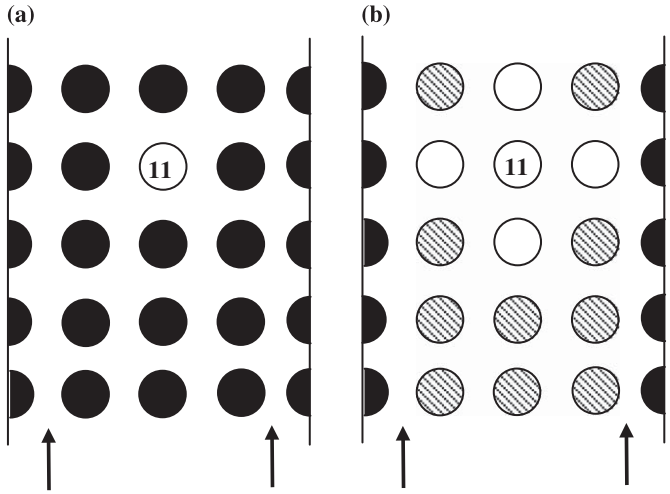

Fig. 7. Instrumented tube locations of (a) single flexible tube in a rigid array; (b) fully flexible array (Solid represents fixed tubes; Hatched tubes in figure 'b' represent flexible tubes that are not monitored during experiments).

determine the onset of instability and to obtain damping ratio measurements as a function of void fraction. Prior experiments were carried out in single phase flow to determine the instability thresholds (Mitra, 2005). Experiments were carried out with a single flexible tube in a rigid array where the central tube (labeled as tube 11) in row 4 of the flexible tube array was monitored as shown in Fig. 7(a). Following this, experiments were carried out with a fully flexible tube array where four neighboring tubes were also monitored as shown in Fig. 7(b). Generally, the increase in amplitude of the tube vibration as the fluid-elastic instability set in was not visually distinct as in the single phase flow runs. However, on post-processing the data, the onset of instability could be determined from the intersection of the slopes of the vibration amplitude.

The summary of the parameters at the onset of instability for all three tube masses for a single flexible tube is listed in Table 3. The critical air flow rate, $V_{g,\mathrm{cr}}$, is listed in the table along with the corresponding critical void fraction. The critical void fraction is measured using the radiation attenuation method. In order to characterize the instability, the frequency of tube vibration in still fluid, f_l, obtained from an impulse response of the tube at the beginning of the test is used. The two-phase density is calculated from the known void fraction and the densities of the individual phases. The total damping ratio, ζ, which includes the structural damping, flow damping and two-phase damping is deduced from the amplitude spectrum of the strain gauge vibration signal just prior to the critical void fraction. The reduced velocity, based on the critical pitch velocity as defined in Eq. (5), and mass damping parameter are calculated according to Eq. (1). Clear transition to instability could not be measured using the strain gauge signal due to malfunction for the aluminum tube at a base liquid velocity of 0.2 m/s and for the stainless steel tube for a base liquid velocity of 0.24 m/s and hence are not reported in Table 3.

Table 3
Parameters at onset of instability in air-water flow (Single flexible tube in a rigid array).

Q_l (gpm)	V_l (m/s)	$V_{g,cr}$ (m/s)	$V_{p,\mathrm{cr}}$ (m/s)	f_l (Hz)	α_{cr}	$\rho_{2\phi}$ (kg/m^3)	ζ (%)	$2\pi m\zeta/\rho D^2$	$V_{p,\mathrm{cr}}/f_l D$
Aluminum tube, $m_a = 0.2$ kg/m									
60	0.24	0.058	1.043	13.3	9.9	898.64	3.8	0.48	4.94
40	0.17	0.132	1.057	13.3	22.3	775.66	4.4	0.59	4.99
Stainless steel tube, $m_a = 0.59$ kg/m									
50	0.20	0.093	1.026	10.09	16.1	837.45	3.4	0.84	6.35
40	0.16	0.139	1.056	10.09	23.2	767.29	4.0	1.02	6.54
Brass rod, $m_a = 1.70$ kg/m									
60	0.24	0.059	1.047	7.5	10.2	896.55	3.1	1.67	8.79
50	0.20	0.105	1.061	7.5	17.6	822.80	3.4	2.00	8.91
40	0.16	0.168	1.148	7.5	27.1	727.92	3.8	2.50	9.64

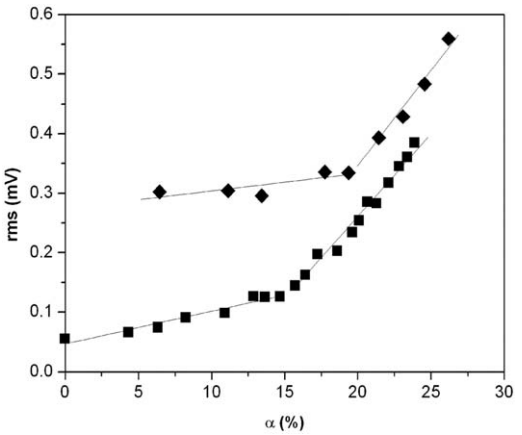

Fig. 8. Vibration amplitude of a single flexible steel tube and a single flexible brass tube in a rigid array as a function of void fraction in air-water flow; $V_l = 0.2$ m/s (■ stainless steel tube; ◆ brass tube).

The rms vibration amplitude signal as a function of the void fraction is shown in Fig. 8 for a single flexible stainless steel tube and a brass tube in a rigid array at a base liquid flow rate of 0.2 m/s. In both cases, the amplitude of vibration starts to increase with an increase of void fraction or gas velocity, and beyond a threshold void fraction, the amplitude increases at a faster rate signaling the onset of instability. The magnitude of vibration amplitude is higher for the brass tube in the stable region. This is attributed to the small amount of slack (loosening) that was introduced in the brass tube-wire system in order to achieve the lower natural frequency as required by Eq. (14). This slack caused the tube to vibrate with larger vibration amplitudes as compared to the taut stainless steel and aluminum tubes for the same excitation impulse. A similar trend is observed for the aluminum tubes and at the higher liquid velocity of 0.24 m/s. At a lower liquid velocity of 0.16 m/s, the transition to instability is not very distinct with the amplitude increasing quite rapidly with an increase in void fraction followed by another change in slope signaling the onset of instability. The larger amplitudes and the increasing slope of the amplitude noticed in the latter case are attributed to the random excitation of the tubes due to the turbulent nature of air-water two-phase flow. This was visually observed while conducting the low liquid velocity runs. The vibration amplitudes as a function of the void fraction for all other cases appear in Mitra (2005).

For the fully flexible array, no systematic differences in the onset of instability were observed as a function of the position of the tubes in the array. In an experimental run, the critical void fraction was determined for all 5 monitored tubes. The averaged value was used to characterize the instability in the Connors criterion. Because of the difficulty in quantifying the effects due to hydrodynamic interaction between surrounding tubes, the damping ratio measured for a single flexible tube surrounded by rigid tubes was used in the calculation of the mass damping parameter. This damping ratio measurement was obtained from the previous test cases of a single flexible tube in a rigid array at a void fraction corresponding to that for which instability is obtained for the fully flexible array case. The parameters at the onset of instability are presented in Table 4. In order to characterize the instability, the frequency of tube vibration of the central tube surrounded by other flexible tubes in still fluid, f_l, is obtained from an impulse response of the tube at the beginning of the test. It is seen that the critical gas velocity required for instability at a particular liquid velocity is lower for the flexible tube array as compared to the single flexible tube. As a result, the damping ratio predicted at the onset of instability is also smaller for a fully flexible array. The rms amplitude of tube vibration of the central tube in the flexible array as a function of void fraction is shown in Fig. 9 for a stainless steel and brass tube at a base liquid velocity of 0.2 m/s. Complete results of the vibration amplitudes for all cases are listed in Mitra (2005).

The effect of the flow velocity and tube mass on the two-phase flow critical void fraction can be discerned by examining the data of Tables 3 and 4. If the critical void fraction is plotted as a function of the nondimensional liquid free-stream velocity, V_l/f_lD, for the three different tube masses, it is found that for a given nondimensionalized liquid velocity; the aluminum tube will require the least amount of gas flow rate to become unstable followed by the stainless steel tube and then the brass rod. The tube masses increase in the same proportion with the aluminum tube being the lightest tube tested and the brass rod the heaviest. This shows that for different tube masses vibrating at the same frequency, and at the same flow velocity, a lighter tube will require the least flow rate of gas to become unstable as compared to a heavier tube. These results are not in agreement with the findings of Weaver and Yeung (1984) who carried out similar tests with acrylic, aluminum and brass tubes, but in single phase liquid flow and found the dimensionless velocity at instability to be the same for all the tubes. They attributed this to the low mass ratios involved where fluid elastic instability apparently has little dependency on the mass damping parameter. It should be noted that

Table 4
Parameters at onset of instability in air-water flow (Fully flexible array).

Q_l (gpm)	V_l (m/s)	$V_{g,\mathrm{cr}}$ (m/s)	$V_{p,\mathrm{cr}}$ (m/s)	f_l (Hz)	α_{cr}	$\rho_{2\phi}$ (kg/m^3)	ζ (%)	$2\pi m\zeta/\rho D^2$	$V_{p,\mathrm{cr}}/f_lD$
Aluminum tube, $m_a = 0.2$ kg/m									
60	0.24	0.043	0.991	13.9	7.6	922.84	3.5	0.43	4.45
40	0.17	0.129	1.047	13.9	22.0	858.54	4.4	0.58	4.71
Stainless steel tube, $m_a = 0.59$ kg/m									
50	0.21	0.08	0.998	10.77	14.1	858.1	3.1	0.78	5.79
40	0.17	0.123	1.026	10.92	21.4	785.4	3.7	1.00	5.87
Brass rod, $m_a = 1.70$ kg/m									
60	0.24	0.052	1.022	7.84	9.0	908.1	2.9	1.52	8.15
50	0.21	0.093	1.059	7.84	15.8	840.91	3.3	1.82	8.44
40	0.17	0.156	1.141	7.84	25.3	745.91	3.8	2.34	9.10

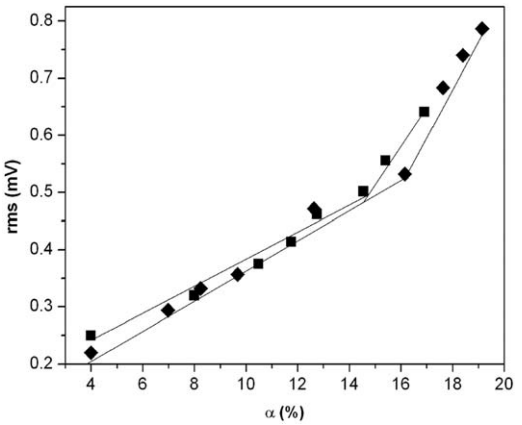

Fig. 9. Vibration amplitude of central flexible steel and brass tube in a fully flexible array as a function of void fraction in air-water flow; $V_l = 0.2$ m/s. (■ stainless steel tube; ◆ brass tube).

the stiffness of the tube systems in their experiments were not matched and varied over a large range. However, the current trend is consistent with the results of Joo and Dhir (1995) who found an effect of the tube mass on the critical velocity. Moreover, an examination of the present data also shows that a fully flexible array becomes unstable at lower void fractions as compared to a single flexible tube surrounded by rigid tubes.

6. Steam-water flow

In order to investigate the effect of the fluid system on the onset of instability, experiments were also carried out with the same setup of tubes in steam-water flow. The main differences between the air-water and steam-water flow properties have been listed in Table 1. The steam-water flow experiments in the current study differ from those of Axisa et al. (1984, 1985), Nakamura et al. (1995) and Hirota et al. (2002) in that they were conducted at much lower pressures and at lower void fractions placing them in the bubbly flow regime. Steam was produced using a combination of a primary heater to heat the water to saturation, and a control heater located in the entrance section upstream of the tube array that was used to supply the latent heat of vaporization to produce steam. The experimental runs were conducted in the same manner as for air-water flow by holding the base liquid free-stream velocity, V_l, constant and then increasing the void fraction of the steam-water mixture until large amplitude vibrations occurred. The steam velocity was determined from the mass quality that was obtained from an energy balance in the test section. The mixture void fraction was measured using the radiation attenuation method.

The parameters at the onset of instability with a single flexible tube are listed in Table 5. The damping ratio at critical void fraction was determined for the case of a single flexible tube as in the air-water two-phase flow cases. The frequency of tube vibration in still fluid, f_l, obtained from an impulse response of the tube at the beginning of the test is used in Table 5. The amplitude of tube vibration is plotted as a function of the void fraction for a stainless steel and brass tube in Fig. 10. Like in the air-water flow cases, two regions with significantly different slopes could be distinguished and the point of intersection of the lines fitted through the data in these regions denoted the instability threshold.

Some clear differences can be pointed out between the steam-water and air-water flow runs. At lower liquid velocities, the amplitude of tube vibration in air-water flow increased at a much faster rate with an increase in void fraction in comparison to the steam-water flow experiments. This can be seen from the slope of the vibration amplitude with respect to void fraction prior to instability for all liquid velocities. Moreover, most experiments show a large and distinct change in slope of the amplitude of vibration after the onset of instability for the steam-water flow experiments.

Table 6 presents the results from the experiments carried out with a fully flexible array in steam-water flow. A clear transition to instability was not measured due to strain gauge malfunction for the stainless steel tubes at a liquid velocity of 0.16 m/s and is not presented here. Once again, the critical void fraction and steam velocity corresponding to the critical void fraction determined from energy balance represent the average values measured for the five monitored tubes. No systematic differences, except those due to the slight differences in the natural frequencies of the tubes, were noticed in the onset of instability of the different tubes. The damping ratio at the critical point was determined from the

Table 5
Parameters at onset of instability in steam-water flow (Single flexible tube).

Q_l (gpm)	V_l (m/s)	$V_{g,cr}$ (m/s)	$V_{p,cr}$ (m/s)	f_l (Hz)	α_{cr}	$\rho_{2\phi}$ (kg/m^3)	ζ (%)	$2\pi m\zeta/\rho D^2$	$V_{p,cr}/f_l D$
Aluminum tube, $m_a = 0.2$ kg/m									
60	0.24	0.084	1.134	13.74	13.8	824.82	3.7	0.48	5.16
50	0.2	0.12	1.12	13.74	20.1	763.96	3.8	0.52	5.09
40	0.16	0.182	1.197	13.74	29.0	679.6	4.1	0.59	5.44
Stainless steel tube, $m_a = 0.59$ kg/m									
60	0.24	0.14	1.33	10.35	20.9	756.32	4.6	1.21	8.03
50	0.2	0.2	1.4	10.35	28.7	681.9	5.2	1.49	8.45
40	0.16	0.272	1.512	10.35	37.1	601.93	5.4	1.70	9.13
Brass rod, $m_a = 1.70$ kg/m									
60	0.24	0.118	1.253	8	18.7	777.91	3.1	1.87	9.79
50	0.2	0.185	1.3475	7.62	27.5	693.55	3.7	2.49	11.05
40	0.16	0.315	1.6625	7.62	40.2	572.31	4.6	3.68	13.64

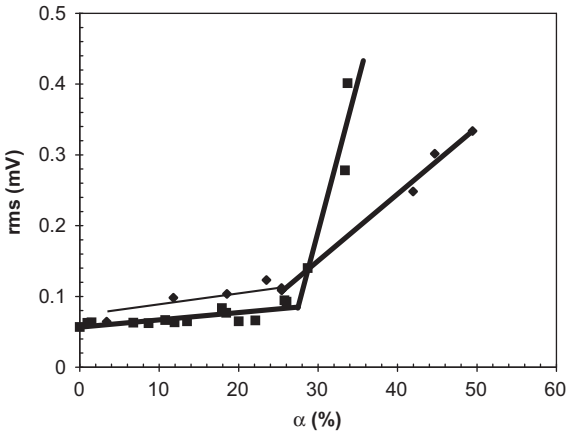

Fig. 10. Vibration amplitude of a single flexible steel and brass tube in a rigid array as a function of void fraction in steam-water flow; $V_l = 0.2$ m/s. (■ stainless steel tube; ◆ brass tube).

correlation developed for the single flexible tube. The frequency of tube vibration of the central tube surrounded by other flexible tubes in still fluid at the beginning of the test is used in Table 6. As expected from the air-water flow experiments, the instability occurred at a slightly lower steam velocity for the fully flexible array in comparison to the case of a single flexible tube in a rigid array for all the liquid velocities.

The tube vibration amplitude of the central tube 11 is shown in Fig. 11 for a stainless steel and brass tube in steam-water flow. It should be noted that for the experiments with the stainless steel tube array, sufficient data points were not available in the region of instability. However, the point of instability was obtained by plotting the best line fit through the available data points. Hence, a greater degree of uncertainty exists for this experiment.

The effect of the flow velocity and tube mass on the two-phase flow critical void fraction can again be discerned by examining the data of Tables 5 and 6. The results obtained are similar to the case of air-water flow indicating that a fully flexible array becomes unstable at a lower void fraction as compared to a single flexible tube and that the critical void fraction increases as the mass of the tube increases.

In an actual steam generator, nucleate boiling is present on the tube surface along with two-phase mixtures surrounding the tubes. It can be expected that the presence of boiling will alter the drag characteristics of the flow across the tube thereby altering the onset of fluid-elastic instability. In an attempt to study the effect of nucleate boiling on the tube surface, a few experiments were carried out in steam-water flow where a single flexible tube with embedded cartridge heaters was used to induce nucleate boiling on the tube surface. The embedded heaters could produce a maximum power of 1000 W, yielding a maximum heat flux of 11.2 W/cm^2. The surface temperature of the tube was

Table 6
Parameters at onset of instability in steam-water flow (Fully flexible array).

Q_l (gpm)	V_l (m/s)	$V_{g,cr}$ (m/s)	$V_{p,cr}$ (m/s)	f_l (Hz)	α_{cr}	$\rho_{2\phi}$ (kg/m^3)	ζ (%)	$2\pi m\zeta/\rho D^2$	$V_{p,cr}/f_l D$
Aluminum tube, $m_a = 0.2$ kg/m									
60	0.24	0.048	1.008	13.74	8.6	874.22	3.3	0.42	4.59
50	0.2	0.111	1.0885	13.74	19.0	774.76	4.0	0.53	4.95
40	0.16	0.131	1.0185	13.74	23.2	734.82	3.7	0.51	4.63
Stainless steel tube, $m_a = 0.59$ kg/m									
60	0.24	0.1074	1.2159	10.59	16.9	794.54	4.0	1.02	7.18
50	0.2	0.142	1.197	10.59	22.4	741.8	4.2	1.13	7.06
Brass rod, $m_a = 1.70$ kg/m									
60	0.24	0.063	1.0605	7.42	10.8	852.82	2.7	1.52	8.93
50	0.2	0.133	1.1655	7.6	21.6	749.63	3.4	2.11	9.58
40	0.16	0.213	1.3055	7.8	32.0	649.99	4.3	3.03	10.46

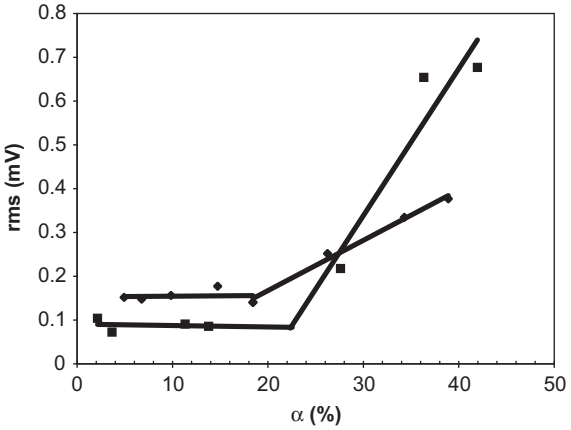

Fig. 11. Vibration amplitude of central flexible steel and brass tube in a fully flexible array as a function of void fraction in steam-water flow; $V_l = 0.2$ m/s. (■ stainless steel tube; ◆ brass tube).

measured to be 109 °C using thermocouples placed on the outer surface of the tube. Similar experiments have been carried out by Gidi et al. (1997) in Freon two-phase flow. They found that boiling actually decreased the amplitude of vibration and also delayed instability. However, they did not attribute this effect to the boiling but due to differences in bubble size, flow regime and void distribution due to vapor being generated on the neighboring tubes. It could be expected that production of bubbles on the tube surface will change the drag characteristics of the surface thereby affecting the fluid-elastic forces acting on the tube.

In order to validate this, single phase flow experiments were also carried out with a single flexible heated tube in a rigid array. In the first experiment, water was heated to a temperature of 100 °C, which was lower than the saturation temperature corresponding to the pressure in the test section. For these experiments, the superficial liquid gap or pitch velocity, V_p, as defined by Eq. (3) is used to characterize the instability In Figs. 12 and 13. Transition to instability was observed at a liquid gap velocity of 0.9 m/s. After this test, the heaters were turned on at maximum power so that the heat flux at the surface of the heaters was 11.2 W/cm^2. It was noticed that the amplitude of vibration of the tube even with no flow increased due to the release of bubbles at the tube surface. As the velocity increased, the amplitude of vibration increased. However, beyond a flow velocity of about 0.7 m/s, the amplitude of vibration decreased very slightly even when the velocity increased to a point where instability had been observed with the unheated tube. The amplitude of vibration only began to increase continuously at a superficial gap velocity of 1.01 m/s indicating that the instability was slightly delayed due to boiling on the tube surface. The vibration amplitude of the tube with ($q = 0$ W/cm^2) and without boiling ($q = 11.2$ W/cm^2) as a function of the gap velocity is shown in Fig. 12. The figure shows that the amplitude of vibration of the heated tube, even at extremely small flow rates is higher for the heated

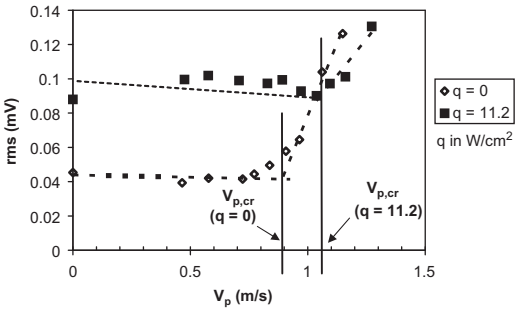

Fig. 12. Onset of instability with and without boiling on tube surface (V_p is the liquid gap velocity).

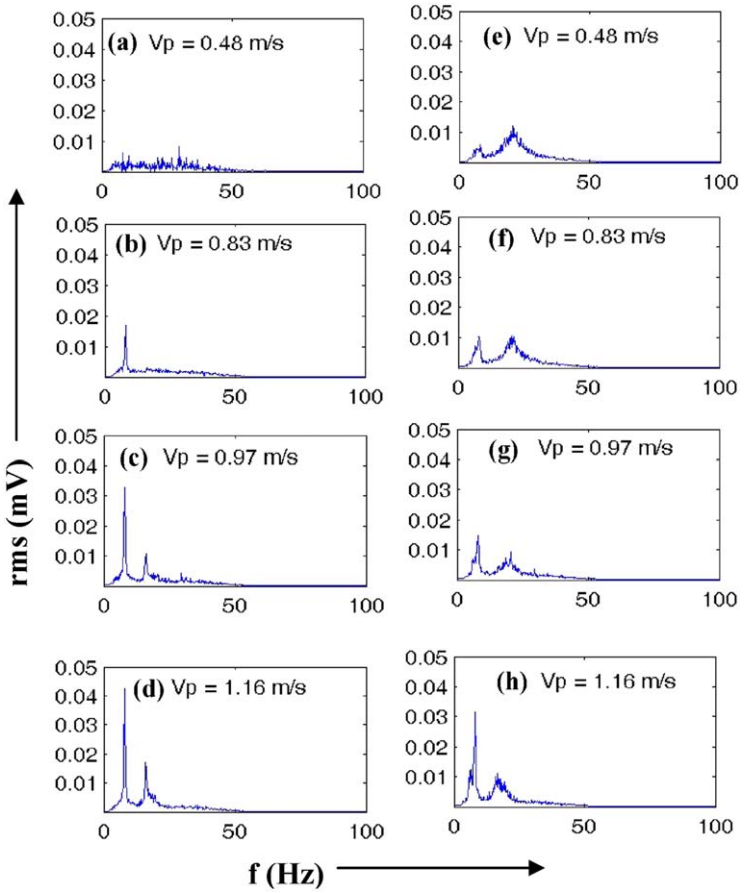

Fig. 13. Amplitude spectrum of vibration signal with heated tube; (a), (b), (c), (d) No boiling on tube surface; (e), (f), (g), (h) Boiling on tube surface (V_p is the liquid gap velocity).

tubes because of the bubbles lifting off from the tube surface. Moreover, it is also seen that the rate of increase of the amplitude after the instability is less steep for the heated tube indicating that boiling on the tube surface acts as a damper to the vibrations. The figure also shows that instability is slightly delayed due to the introduction of vapor on the tube surface and that the relative increase in the amplitude of the tube vibration is much steeper without boiling on the tube surface. These trends are in agreement with the findings of Gidi et al. (1997).

An interesting phenomenon was observed in the amplitude spectrum of the tube vibration signal with and without boiling on the tube surface, which is shown in Fig. 13 at different superficial gap velocities. With boiling on the tube

Table 7
Instability parameters without and with boiling on tube surface (single flexible tube in a rigid array).

Q_l (gpm)	V_l (m/s)	$V_{g,cr}$ (m/s)	$V_{p,cr}$ (m/s)	f_l (Hz)	α_{cr}	$\rho_{2\phi}$ (kg/m^3)	ζ (%)	$2\pi m\zeta/\rho D^2$	$V_{p,cr}/f_l D$
No nucleate boiling on tube surface									
60	0.24	0.20	1.54	8.2	27.1	697.17	4.7	2.55	11.74
50	0.20	0.275	1.66	8.2	34.92	622.64	4.7	2.80	12.65
40	0.16	0.33	1.70	8.2	40.8	566.38	5.3	3.48	12.96
Nucleate boiling on tube surface									
60	0.24	0.23	1.645	8.2	29.3	676.36	4.8	2.67	12.54
50	0.20	0.3	1.75	8.2	37.5	598.1	4.9	3.07	13.34
40	0.16	0.37	1.855	8.2	42.89	546.66	5.5	3.71	14.14

surface, the amplitude spectrum at any given superficial gap velocity shows two distinct frequency peaks. The lower frequency peak at 8.1 Hz corresponds to the natural frequency of the heated tube assembly. The second peak is much broader and occurs at approximately the first harmonic. This is attributed to the rocking motion of the tube caused by bubbles being released from the surface due to nucleate boiling. At extremely small flow rates, the peak at the first harmonic dominates indicating that the vibration is mainly due to bubble release from the tube surface. As the flow rate increases, the peak due to the natural frequency becomes comparable to that due to bubble release. After the instability sets in at 1.04 m/s, the peak corresponding to the natural frequency increases in magnitude and becomes sharper, indicating the onset of fluid-elastic instability.

Two-phase flow experiments with boiling on the tube surface were carried out with a single flexible heated tube in a rigid array of unheated tubes with bulk steam production upstream of the tube bundle. After establishing steam-water flow at a base void fraction, the heater on the central flexible tube in a rigid array was turned on such that additional vapor was produced on the tube surface. Experiments were carried out in the same manner as the steam-water flow experiments by holding the base freestream liquid flow velocity constant and gradually increasing the void fraction. Once the void fraction was established, the vibration amplitude was recorded without heating on the tube surface and then followed by nucleate boiling on the tube surface. The parameters at the onset of fluid-elastic instability without and with boiling on the tube surface are presented in Table 7. The damping ratio at the onset of instability in the case of heating on the tube surface is determined from the measurements made with no boiling on the tube surface. The table clearly indicates the higher void fractions required to reach instability with boiling on the tube surface, which is again in agreement with the experiments of Gidi et al. (1997).

7. Discussion

The results of the experiments with air-water and steam-water flow showed that a fully flexible array becomes unstable at a lower void fraction in two-phase flow when compared to a single flexible tube surrounded by a rigid array. This section mainly focuses on the differences between the different arrays and between air-water and steam-water flow.

The Connors criterion for different tube arrays is plotted using the corresponding mass damping parameters and the reduced velocities as listed in Tables 3–6. Since the stiffness of the different tube systems is held approximately constant, a single fit can be made through the data points of the three different masses since the instability constant is a function of the tube stiffness. A fit through each individual data series consisting of data points of tubes with the same mass is also made.

A plot of Connors' criterion for the air-water flow experiments is shown for the single flexible tube in a rigid array and for a fully flexible array in Fig. 14. A fit through the data points for the single flexible tube yields an instability constant, $K = 6.5$. The dotted lines show the limits of the 95% confidence interval. It is seen that most of the data points lie within the envelope indicating a satisfactory fit of the data. The best fit for the fully flexible array yields a value of $K = 6.2$. Fig. 14 also shows that the stability boundary for a fully flexible array is lower than that for a single flexible tube. This suggests that a design criterion based on the experiments for a flexible tube in a rigid array is not conservative in terms of predicting fluid-elastic instability. It should also be noted that a data fit through points consisting of tubes of the same mass (each figure shows three such data fits for the aluminum, stainless steel and brass tubes) shows a very different trend when compared to Connors' criterion. The change in mass ratio for the data series consisting of tubes with the same mass is mainly due to variations in void fractions.

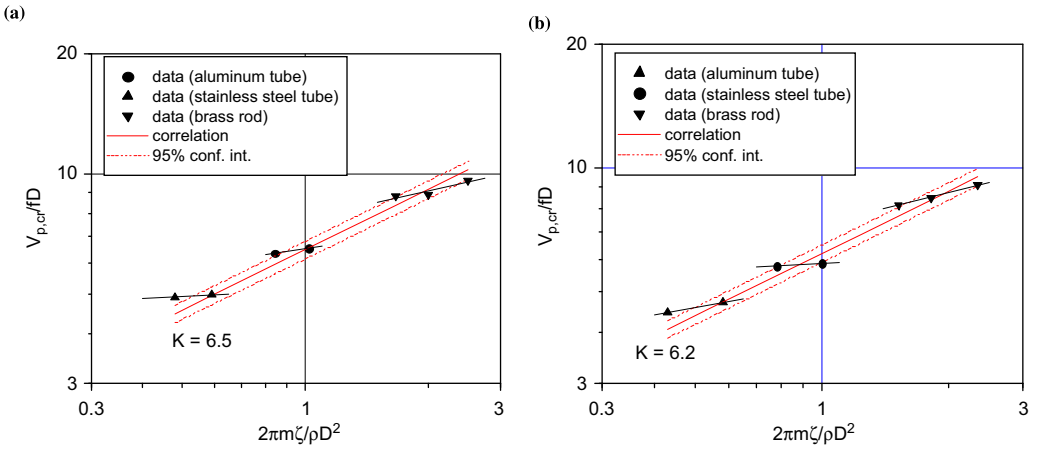

Fig. 14. Connors' criterion plot for air-water two-phase flow experiments (a) Single flexible tube in a rigid array; (b) Fully flexible array.

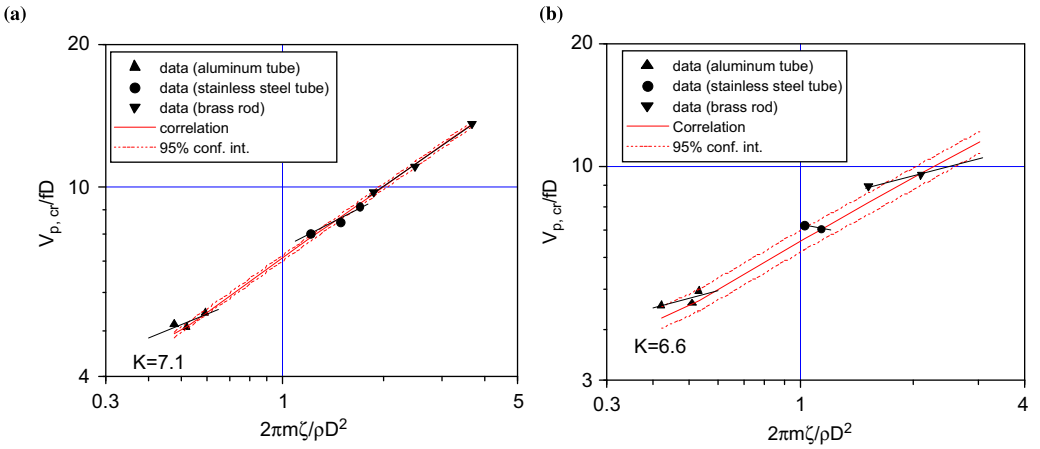

Fig. 15. Connors' criterion plot for steam-water two-phase flow experiments (a) Single flexible tube in a rigid array; (b) Fully flexible array.

The experiments in steam-water flow provide some much needed data in this area, especially at low pressures. Visual observation showed that a steam-water mixture was a lot less turbulent than the corresponding air-water mixtures. Connors' criterion for a single flexible tube and a fully flexible array in steam-water flow are shown in Fig. 15. The best fit line for a single flexible array yields an instability constant of 7.1 for the single flexible tube and a value of 6.6 for the fully flexible array. As expected, a comparison of the correlations in steam-water flow also shows that the fully flexible array is less stable as compared with the single flexible tube using Connors' criterion.

The experiments carried out with air-water and steam-water flow in the same test section with exactly the same tube systems makes it possible to compare the performance of the two systems with respect to fluid-elastic instability. The data from Tables 3–6 reveal that for the same liquid superficial freestream velocity, the void fraction required for instability is higher in steam-water flow as compared to air-water flow. The same conclusion is drawn by plotting the correlations based on Connors' criterion. Fig. 16 shows the plot of Connors' criterion for a single flexible tube and a fully flexible array in both air-water and steam-water flow. It can clearly be seen that for the same mass damping parameter, a tube in steam-water flow requires a higher velocity to reach the instability. This effect was not observed by Axisa et al. (1985) who did not notice any difference between the steam-water and air-water flow experiments in terms of the onset of instability when plotted using Connors' criterion. However, differences in the properties of the fluid systems such as the density ratio, surface tension, viscosity and thermal diffusivity have been pointed out by a number of investigators (Pettigrew et al., 2002; Feenstra et al., 2002) and hence a change in the fluid-elastic forces can be

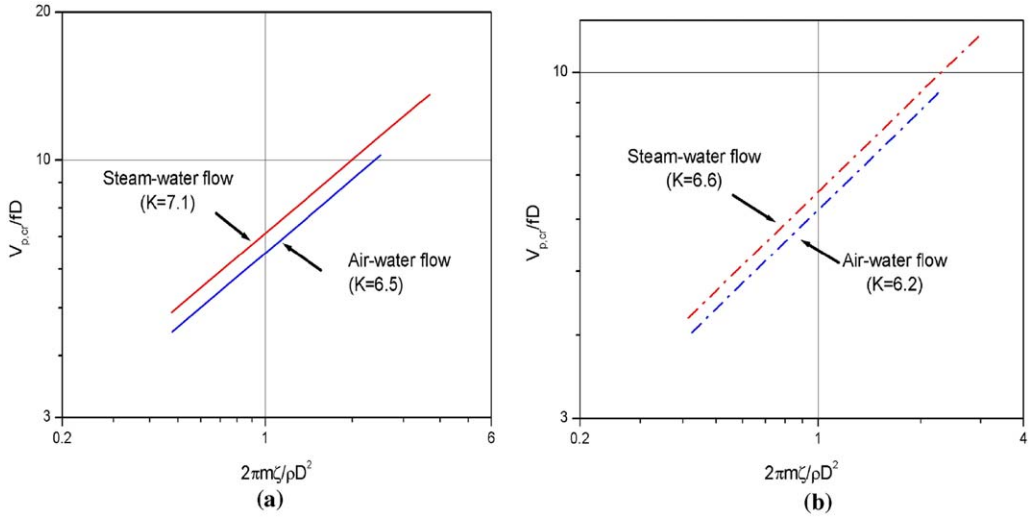

Fig, 16. Comparison of Connors' criteria in air-water and steam-water flow (a) Single flexible tube; (b) Fully flexible array.

Table 8
Experimental details of different air-water two-phase fluid-elastic instability experiments.

Attribute	Pettigrew et al. (1989)	Joo and Dhir (1995)	Heilker and Vincent (1981)	Present study
Array Geometry	Normal square	Normal triangular	Parralel triangular	Normal square
P/D range	1.32, 1.47	1.4	1.44	1.4
Void fraction (%) range	5–99	0–50	0–80	0-40
Method of suspension	Cantilevered at end	Cantilever-beam sus.	Cantilevered at end	Piano wire
Supported ends	One end	Both ends	One end	Both
Rigid/Flex. array	Fully flexible array	Flexible tube/Rigid array	Fully flexible array	Fully flexible array
L/D	46	9	41	7.25

expected based on these differences in fluid thermophysical properties. Effects due to the drag experienced on the tubes in the two fluid systems could also have an effect on the instability. Another difference is the possibility of state change of the two-phase mixture induced by vibrations or thermohydraulics. Steam-water and other liquid-vapor mixtures would demonstrate this effect whereas phase change will not occur in air-water systems. This phenomenon needs to be investigated further.

8. Comparison with existing data

Two-phase fluid-elastic instability data is not as abundant as for single-phase flow. Moreover, most of the two-phase flow experiments have been carried out in air-water flow. A handful of researchers have conducted experiments in steam-water flow and freon. However, two-phase flow data reported in the literature do not differentiate between the types of tube support conditions used in the experiments. The effect of the pitch-to-diameter ratio is understood through correlations proposed by Pettigrew et al. (1989). Often, differences also exist in the method of calculation of the instability parameters. Here, the results of the present study are compared with data of several other researchers. Table 8 lists the characteristics of the different data series in air-water flow used for the comparison. The experiments of Pettigrew et al. (1989) were conducted with cantilevered tubes arranged in normal square, normal triangular and

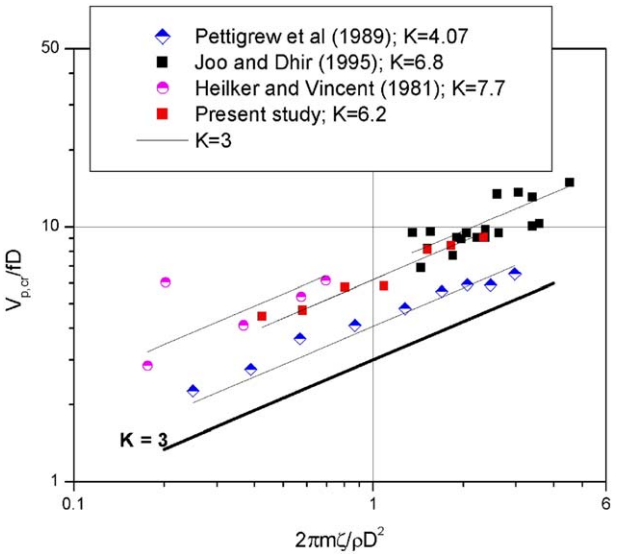

Fig. 17. Comparison of air-water two-phase flow data with other researchers.

rotated triangular arrays. The experiments with the normal square array are compared here. Heilker and Vincent (1981) conducted experiments with a parallel triangular array where the tubes were supported from their ends using O-rings simulating pinned end conditions. The experiments of Joo and Dhir (1995) were conducted with tubes suspended using thin stainless steel strips. The present study was carried out using tubes suspended from piano wires. All the experiments except Joo and Dhir's (1995) were carried out with fully flexible arrays. In making the comparison, measured void fraction is used in the calculation of the density. Some of the earlier works (Pettigrew et al., 1989) used the superficial void fraction to characterize the instability. This quantity was calculated as

$$\beta = \frac{V_g}{V_g + V_l}. \tag{15}$$

For comparison to the present study, their void fraction was recalculated assuming that a drift flux correlation (Eqs. (9), (10) and (11)) could adequately predict the actual void fraction. The stiffness of the different tube systems in air was calculated knowing the natural frequency of the tubes in air and their respective masses. The results are plotted in Fig. 17. The figure shows that the experiments of Pettigrew et al. (1989) have the lowest instability bound, yielding an instability constant $K = 4.07$. The present study ($K = 6.2$) and the experiments of Joo and Dhir (1995) ($K = 6.8$) yield almost the same instability constant. Finally, Heilker and Vincent's (1981) data ($K = 7.7$) yields the highest instability constant due to low damping values measured near instability.

The experiments of Pettigrew et al. (1995) and Feenstra et al. (2002) were carried out in Freon flow, whereas the experiments of Hirota et al. (2002), Axisa et al. (1985) and the present study were carried out in steam-water flow. In the present study and the study of Hirota et al. (2002), tubes were suspended using piano wires while Pettigrew et al. (1995) and Feenstra et al. (2002) used cantilevered tubes. Axisa et al. (1985) used tubes that were clamped at both ends. Table 9 shows the experimental conditions for the various steam-water and freon flow cases considered. Once again, measured void fractions were used in plotting the data of the present study and that of Feenstra et al. (2002), and a drift flux correlation was used to estimate the actual void fraction for the data of the other researchers. Of special interest are the data of the present experiments with a single flexible tube and that of Hirota et al. (2002), which were conducted with similar suspension methods and normal square arrays. Fig. 18 shows the comparison of the present steam-water data with the data from other sources. It is seen that the data of Hirota et al. (2002) and the present study collapse onto each other with almost same instability constants, $K = 7.1$ for the present study and $K = 7.2$ for Hirota et al. (2002). Similarly, the data of Feenstra et al. (2002) and Pettigrew et al. (1995) are clustered near the bottom with similar instability constants. The data of Axisa et al. (1985) with the highest stiffness also correspond to the largest instability constant. The void fraction of the two-phase mixture was limited to below 40% in the present experiments placing the flows in the bubbly regime. Some of the results in literature exhibit deviation from Connors' criterion due to transition from bubbly to intermittent flow regime. Some differences in Figs. 17 and 18 could possibly due to this effect.

Table 9
Experimental details of different steam-water and freon two-phase fluid-elastic instability experiments.

Attribute	Pettigrew et al. (1995)	Feenstra et al. (2002)	Hirota et al. (2002)	Axisa et al. (1985)	Present study
Fluid	R-22	R-11	Steam-water	Steam-water	Steam-water
Array Geometry	Parallel triangular	Parallel triangular	Normal square	Normal square	Normal square
P/D range	1.5	1.44	1.46	1.44	1.4
Void fraction (%) range	0–65	0–80	70–96	85 – 98	0-40
Method of suspension	Cantilevered at end	Cantilevered at end	Piano wire	Cantilevered at end	Piano wire
Supported ends	One end	One end	Both ends	Both ends	Both ends
Rigid/Flex. array	Fully flexible array	Fully flexible array	Flexible tube/ Rigid array	Fully flexible array	Fully flexible array
L/D	48 (long)	48 (long)	7.25 (long)	62.5 (long)	7.25 (long)

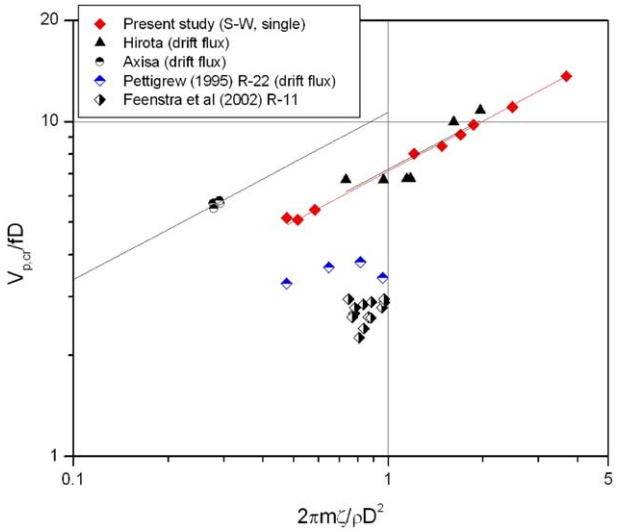

Fig. 18. Comparison of current steam-water two-phase flow data with other researchers (steam-water and freon).

9. Conclusions

The main conclusions drawn from the current work are as follows.

(i) Single phase and two phase flow experiments with tubes of different masses tuned to a frequency such that the stiffness of the tube systems were approximately same showed that for the same base free-stream velocity of the liquid phase, the lightest tube became unstable at the lowest void fraction, and that the critical void fraction for fluid-elastic instability was generally proportional to the tube masses.
(ii) The single phase and two-phase flow experiments also showed that tubes in a fully flexible array become unstable at lower flow velocities as compared to a single flexible tube surrounded by rigid tubes.
(iii) The fluid-elastic instability threshold in steam-water flow is found to be higher than that for air-water flow indicating that tubes are more stable in steam-water flow as compared to air-water flow.

(iv) Nucleate boiling on the surface of the tube in single phase flow is found to delay the onset of fluid-elastic instability and also suppress the amplitude of vibration. Nucleate boiling in two phase steam water flow at the heat fluxes tested in the present work are found to further stabilize the tube vibration by a very small amount.
(v) Two-phase flow experiments in the present study were conducted in the bubbly flow regime with the void fraction limited below 40%.

Acknowledgments

This work was supported by a United States Department of Energy Nuclear Engineering Research Initiative (NERI) grant.

References

Adinolfi, P., 2003. Multiple tube fluid elastic instability measurements methods and experimental data. Masters' Thesis, University of California, Los Angeles.

Axisa, F., Villard, B., Gilbert, R.J., Hestroni, G., Sundheimer, P., 1984. Vibration of tube bundles subjected to air-water and steam-water cross flow: preliminary results on fluidelastic instability. In: Proceedings of Flow-Induced Vibration, ASME Winter Annual Meeting: New Orleans, pp. 269–284.

Axisa, F., Villard, B., Gilbert, R.J., Boheas, M.A., 1985. Vibration of tube bundles subjected to steam-water cross flow: a comparative study of square and triangular pitch arrays. In: Transactions of the 8th International Conference on Structural Mechanics in Reactor Technology, Vol. B., Brussels, pp. 7–12.

Chen, S.S., Jendrzejcyk, J.A., 1981. Experiments on fluid elastic instability of tube banks subjected to liquid cross flow. Journal of Sound and Vibration 78, 355–381.

Connors Jr., H.J., 1970. Fluidelastic vibration of tube arrays excited by cross flow. In: In Flow Induced Vibration in Heat Exchangers (ed. D.D. Reiff) ASME, New York, pp. 42–56.

Feenstra, P.A., Weaver, D.S., Judd, R.L., 2000. An improved void fraction model for two-phase cross-flow in horizontal tube bundles. International Journal of Multiphase Flow 26, 1851–1873.

Feenstra, P.A., Weaver, D.S., Judd, R.L., 2002. Modelling two-phase flow-excited damping and fluidelastic instability in tube arrays. Journal of Fluids and Structures 16 (6), 811–840.

Feenstra, P.A., Weaver, D.S., Nakamura, T., 2003. Vortex shedding and fluid-elastic instability in a normal square tube array excited by two-phase cross-flow. Journal of Fluids and Structures 17, 793–811.

Gidi, A, Weaver, D.S, Judd, R.L., 1997. Two-phase flow induced vibrations of tube bundles with tube surface boiling. In: Proceedings of the ASME Conference on Fluid-Structure Interaction, Aeroelasticity, Flow-Induced Vibration and Noise, Volume II, pp. 381–389.

Heilker, W.J., Vincent, R.Q., 1981. Vibration in nuclear heat exchangers due to liquid and two-phase flow. ASME Journal of Engineering for Power 103, 358–366.

Hirota, K., Nakamura, T., Kasahara, J., Mureithi, N.W., Kusakabe, T., Takamatsu, H., 2002. Dynamics of an in-line tube array subjected to steam-water cross-flow. Part III: Fluidelastic instability tests and comparison with theory. Journal of Fluids and Structures 16 (2), 153–173.

Ishii, M., Zuber, N., 1979. Drag coefficient and relative velocity in bubbly, droplet or particulate flows. AIChE Journal 25 (5), 843–855.

Joo, Y., 1994. An Experimental Study on Fluidelastic Instability and Drag Force on a Tube in Two-Phase Cross Flow. PhD Thesis, University of California, Los Angeles.

Joo, Y., Dhir, V.K., 1994. An experimental study of drag on a single tube and on a tube in an array under two-phase cross flow. International Journal of Multiphase Flow 20, 1009–1019.

Joo, Y., Dhir, V.K., 1995. On the mechanism of fluidelastic instability of a tube placed in an array subjected to two-phase crossflow. ASME Journal of Fluids Engineering 117, 706–712.

Lever, J.H., Weaver, D.S., 1986. On the stability of heat exchanger tube bundles, Part II: Numerical results and comparison with experiments. Journal of Sound and Vibration 107 (3), 393–410.

Mitra, D.R., 2005. Fluid-elastic instability in tube arrays subjected to air-water and steam-water cross flow. PhD Thesis, University of California, Los Angeles.

Mureithi, N.W., Nakamura, T., Hirota, K., Murata, M., Utsumi, S., Kusakabe, T., Takamatsu, H., 2002. Dynamics of an in-line tube array subjected to steam-water cross-flow. Part II: Unsteady fluid forces. Journal of Fluids and Structures 16 (2), 137–152.

Nakamura, T., Fujita, K., Kawanishi, K., Yamaguchi, N., Tsuge, A., 1995. Study of the vibrational characteristics of a tube array caused by two-phase flow. Part II: Fluidelastic vibration. Journal of Fluids and Structures 9, 539–562.

Nakamura, T., Hirota, K., Tomomatsu, K., Kasahara, J., Takamatsu, H., 1999. On positional effect of flexible tubes in a square array subjected to Freon two-phase flow. In: Proceedings of the ASME PVP Symposium, PVP Vol 389: Flow Induced Vibration, Boston, pp. 73–80.

Nakamura, T., Hirota, K., Watanabe, Y., Mureithi, N.W., Kusakabe, T., Takamatsu, H., 2002. Dynamics of an in-line tube array subjected to steam-water cross-flow. Part I: Two-phase damping and added mass. Journal of Fluids and Structures 16 (2), 123–136.

Pettigrew, M.J., Tromp, J.H., Mastorakos, J., 1985. Vibration of tube bundles subjected to two-phase cross-flow. ASME Journal of Pressure Vessel Technology 107, 335–343.

Pettigrew, M.J., Tromp, J.H., Taylor, C.E., Kim, B.S., 1989. Vibration of tube bundles in two-phase cross-flow: Part 2–fluid-elastic instability. ASME Journal of Pressure Vessel Technology 111, 478–487.

Pettigrew, M.J., Taylor, C.E., 1991. Fluidelastic instability of heat exchanger tube bundles: Review and design recommendations. ASME Journal of Pressure Vessel Technology 113, 242–256.

Pettigrew, M.J., Taylor, C.E., 1994. Two-phase flow-induced vibration: An overview. ASME Journal of Pressure Vessel Technology 116, 233–253.

Pettigrew, M.J., Taylor, C.E., Jong, J.H., Currie, I.G., 1995. Vibration of a triangular tube bundle in two-phase Freon cross flow. ASME Journal of Pressure Vessel Technology 117 (4), 321–329.

Pettigrew, M.J., Taylor, C.E., Fisher, N.J., Yetisir, M., Smith, B.A.W., 1998. Flow-induced vibration: recent findings and open questions. Nuclear Engineering and Design 185, 249–276.

Pettigrew, M.J., Taylor, C.E., Kim, B.S., 2001. The effects of bundle geometry on heat exchanger tube vibration in two-phase cross flow. ASME Journal of Pressure Vessel Technology 123, 414–420.

Pettigrew, M.J., Taylor, C.E., Janzen, V.P., Whan, T., 2002. Vibration behavior of rotated triangular tube bundles in two-phase cross flows. ASME Journal of Pressure Vessel Technology 124, 144–153.

Remy, F.N., 1982. Flow induced vibration of tube bundles in two-phase cross flow. In: Proceedings of the 3rd International Conference on Vibration in Nuclear Plants 1, United Kingdom, pp. 135–160.

Schroder, K., Gelbe, H., 1999. New design recommendations for fluidelastic instability in heat exchanger tube bundles. Journal of Fluids and Structures 13, 361–379.

Weaver, D.S., Yeung, H.C., 1984. The effect of tube mass on the flow induced response of various tube arrays in water. Journal of Sound and Vibration 93 (3), 409–425.

Weaver, D.S., Fitzpatrick, J.A., 1988. A review of cross-flow induced vibrations in heat exchanger tube arrays. Journal of Fluids and Structures 2, 73–93.

Weaver, D.S., Ziada, S., Au-Yang, M.K., Chen, S.S., Paidoussis, M.P., Pettigrew, M.J., 2000. Flow-induced vibrations in power and process plant components –progress and prospects. ASME Journal of Pressure Vessel Technology 122, 339–348.